Journal of Hazardous Materials 166 (2009) 445–454

Contents lists available at ScienceDirect

Journal of Hazardous Materials

journal homepage: www.elsevier.com/locate/jhazmat

Ablation mechanism of polymer layered silicate nanocomposite heat shield

Ahmad Reza Bahramian, Mehrdad Kokabi*

Polymer Engineering Group, Chemical Engineering Department, Faculty of Engineering, Tarbiat Modares University, P.O. Box 14115-143, Tehran, Islamic Republic of Iran

ARTICLE INFO

Article history:
Received 26 April 2008
Received in revised form
14 September 2008
Accepted 18 November 2008
Available online 27 November 2008

Keywords:
Heat shields
Ablative nanocomposite
Inverse analysis
Ablation mechanism

ABSTRACT

Recent advances in polymer layered silicate nanocomposites especially improve flammability resistance; encourage the examination of this unique class of evolving materials as potential ablatives. Polymer layered silicate nanocomposites show excellent potential as ablative heat shields. Determining the thermal diffusivity together with the mass and energy transfer is an important problem encountered in design of heat shield system which pyrolyses and ablates at high temperature. The aim of this work is to give information on the influence of the experimental conditions to the estimated effective thermal diffusivity of ablative nanocomposite and composite materials. Here, we present the inverse solution to estimate the parameter used to identify the effective thermal diffusivity of resol type phenolic resin-asbestos cloth montmorillonite layered silicate nanocomposite and its composite counterpart. The experimental setup consists of a standard oxyacetylene flame test. The transient temperature measurements, taken from the top surface and through the thickness of the samples, are used in the inverse analysis to estimate the change of the effective thermal diffusivity. The results of this work clarify the mechanism of the ablation and thermal diffusivity of the layered silicate nanocomposite heat shields due to the high temperature degradation in comparison with its composite counterpart.

1. Introduction

The term nanocomposite describes a two-phase material where one of the phases has at least a dimension less than 100 nanometer [1–3]. Polymer layered silicate nanocomposites belong to a class where the reinforcing phase, in the shape of platelets, has a thickness in nano scale [3–6]. Polymer nanocomposites are of great industrial as well as academic interest. From the academic side, a new scale is available in intermediate between molecular and micro-scales [7,8]. The potential for more sophisticated tailoring of properties is apparent. From the industrial point of view, the major interest is in the dramatically improved properties [9,10].

Recent advances in thermoset resin layered silicate nanocomposites especially improve flammability resistance; encourage the examination of this unique class of evolving material as potential ablatives [10,11]. Thermoset polymer layered silicate nanocomposites show excellent potential as ablative materials because upon pyrolysis, the organic–inorganic nanostructure reinforcing the polymer can be converted into a uniform ceramic layer which may lead to significantly increased resistance to oxidation and mechanical erosion compared to composite ablative materials [11–14].

In this work the ablative performance, thermal decomposition and temperature distribution through the thickness of phenolic resin/asbestos cloth/layered silicate nanocomposite are examined and compared with its phenolic resin/asbestos cloth composite counterpart. The main objective of this study is to open a new window in estimating the effective thermal diffusivity of ablative nanocomposite and composite materials using thermal analysis technique and oxyacetylene flame test.

2. Mathematical model of ablation and thermal degradation

2.1. Mathematical model of ablation

When the ablative sample is exposed to high temperature and high velocity fluid stream, decomposition of resin begins at pyrolysis temperature, and subsequently char layer ablation occurs at higher temperature [15–18]. The free surface of the sample under the influence of high temperature stream is continuously spilled. Therefore, three zones are formed (Fig. 1): the virgin material, the pyrolysis zone and the porous char layer [11,15,18]. The char layer in nanocomposite samples is a dense ceramic layer [11].

In this section, the mathematical model illustrating the thermal decomposition and ablation is described. The main assumptions on which the model rests are listed below [17–23]:

* Corresponding author. Tel.: +98 21 8801 1001; fax: +98 21 8800 6544.
E-mail address: mehrir@modares.ac.ir (M. Kokabi).

0304-3894/$ – see front matter © 2008 Elsevier B.V. All rights reserved.
doi:10.1016/j.jhazmat.2008.11.061

Nomenclature

A	frequency factor (s^{-1})
A_c	frequency factor for char formation (s^{-1})
A_g	frequency factor for gas formation (s^{-1})
c	heat capacity ($J\,kg^{-1}\,K^{-1}$)
c_g	heat capacity of the gas ($J\,kg^{-1}\,K^{-1}$)
E	activation energy of thermal degradation ($J\,mol^{-1}$)
E_c	activation energy for char formation ($J\,mol^{-1}$)
E_g	activation energy for gas formation ($J\,mol^{-1}$)
G	mass rate of gaseous products of thermo-decomposition ($kg\,s^{-1}\,m^{-2}$)
h	heat convection coefficient ($J\,m^{-2}\,K\,s^{-1}$)
ΔH_p	heat of ablation ($J\,kg^{-1}$)
I	enthalpy of surrounding hot gas ($J\,kg^{-1}$)
k	rate constant (s^{-1})
K	thermal conductivity ($J\,m^{-1}\,s^{-1}\,K^{-1}$)
L_0	initial thickness of sample (m)
m_0	initial mass of sample (kg)
m_p	specific pyrolysis mass flow rate ($kg\,m^{-2}\,s^{-1}$)
$m(t)$	mass of sample at time t (kg)
Ma	molecular weight of undissociated air
M_v	average molecular weight of injected vapor
n	degree of thermal degradation
N	transpiration factor
p	transpiration coefficient
q_0	zero heat flux ($J\,s^{-1}\,m^{-2}$)
q_{bL}	the convective heat flux carried off from the heated surface at the expense of injection into the boundary layer of gaseous products of the thermo-decomposition ($J\,s^{-1}\,m^{-2}$)
q_e	the convective heat flux carried off from the surrounding into the surface ($J\,s^{-1}\,m^{-2}$)
q_K	the heat flux consumed for warming sample due to heat conduction ($J\,s^{-1}\,m^{-2}$)
q_{rw}	the radiation heat flux carried off from the surface at the expense of own radiation of the surface ($J\,s^{-1}\,m^{-2}$)
q_w	the convective heat flux carried off from the heated surface heated up to temperature T_w into the surrounding ($J\,s^{-1}\,m^{-2}$)
R	universal gas constant ($J\,kg^{-1}\,mol^{-1}\,K^{-1}$)
s_1	char moving boundary (m)
s_2	pyrolysis moving boundary (m)
S	the cross-section surface area of circular sample (m^2)
t	time (s)
T	absolute temperature (K)
T_0	initial temperature (K)
T_e	hot gas temperature (K)
T_p	pyrolysis temperature (K)
T_w	surface temperature (K)
ΔT_p	temperature difference between initial and final thermal degradation in TG analysis (K)
v_s	velocity of the top surface ($m\,s^{-1}$)
V_{gas}	the mass fraction of the resin transformed to the gas in respect to the mass of sample
X_g	the mass fraction of the resin which may be decomposed in respect to the total mass of resin
y	distance (m)
y_c	yield of charring

Greek letters

α_{eff}	effective thermal diffusivity ($m^2\,s^{-1}$)
δ_B	a thin surface layer of thickness that produces the bubbles (m)
ε	emission factor
ϕ	expansion coefficient
γ_{bl}	transpiration number
ν_2	volumetric concentration of polymer in the sample matrix
ρ	density of the sample ($kg\,m^{-3}$)
ρ_3	density of the char ($kg\,m^{-3}$)
σ	Stefan Boltzmann constant ($J\,m^{-2}\,K^{-4}$)
ζ	Landau transformation

(i) No energy is transferred by mass diffusion.
(ii) Movement of liquid is assumed negligible compared to pyrolysis gases.
(iii) Pyrolysis gases may be considered 'ideal gases' but their properties will be kept constant.
(iv) Volatiles escape from the solid as soon as they are formed from the polymer.
(v) Thermal conductivity of each element of samples is assumed constant.
(vi) The decomposition of polymer occurs in a single step and exhibits a first order reaction.

Hence, the problem can be expressed by the following transient partial differential heat conduction equation [15,21]:

$$\rho c\frac{dT}{dt}+\Delta H_p\frac{d\rho}{dt}+c_g m_p\frac{\partial T}{\partial y}=\frac{\partial}{\partial y}\left(K\frac{\partial T}{\partial y}\right) \tag{1}$$

In this work, the inverse solution technique was employed to determine the nanocomposite ablation mechanism, also to investigate its thermophysical properties changes due to high temperature degradation. For this purpose, equation (1) should be changed to a parameter reduction form, using the following transformations:

$$\frac{d}{dt}=\frac{\partial}{\partial t}+v_s\frac{\partial}{\partial y}$$
$$\frac{d\rho}{dt}=\frac{d\rho}{dT}\cdot\frac{dT}{dt} \tag{2}$$

By combining the Eqs. (1) and (2), we have:

$$\left(\rho c+\Delta H_p\frac{d\rho}{dT}\right)\frac{\partial T}{\partial t}+\left[c_g m_p+v_s\left(\rho c+\Delta H_p\frac{d\rho}{dT}\right)\right]\frac{\partial T}{\partial y}=K\frac{\partial^2 T}{\partial y^2} \tag{3}$$

It can be defined that:

$$\Psi(T)=\rho c+\Delta H_p\frac{d\rho}{dT}$$
$$H(T,v_s)=c_g m_p+v_s\Psi(T)$$
$$\frac{K}{\Psi(T)}=\alpha_{eff}(T)$$
$$Bi=\frac{H(T,v_s)s_1(t)}{K} \tag{4}$$

In these equations, we introduce $\alpha_{eff}(T)$ as an effective thermal diffusivity parameter and Bi as a dimensionless number. Bi is used in unsteady (transient) state as a ratio of convection to conduction heat transfer which is very similar to Biot number.

Therefore, we can rewrite Eq. (1) as follows:

$$\frac{1}{\alpha_{eff}}\frac{\partial T}{\partial t}+\frac{Bi}{s_1(t)}\frac{\partial T}{\partial y}=\frac{\partial^2 T}{\partial y^2} \tag{5}$$

We solve the ablation equation (Eq. (5)) using a front–fixing method and explicit finite difference, where the moving front is

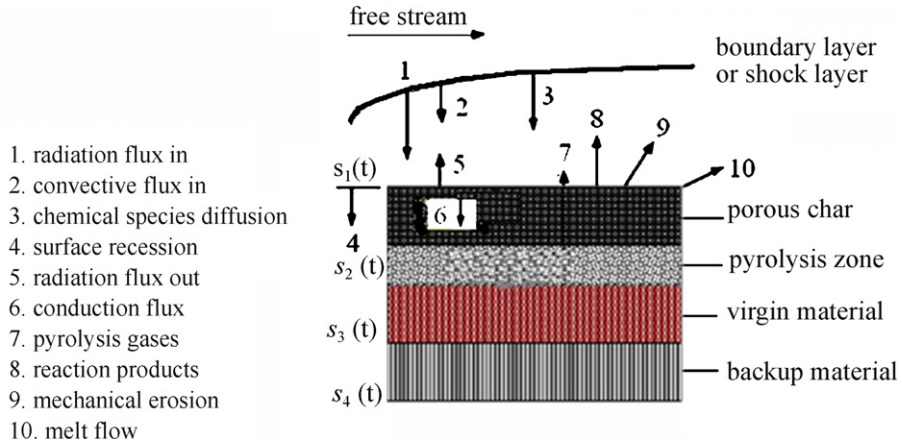

Fig. 1. The zones within the ablating sample [16,20].

made stationary by the Landau transformation [16,21]:

$$\xi = \frac{y - s_1(t)}{L_0 - s_1(t)} \tag{6}$$

The ablation model involves three zones and two moving boundaries, s_1 and, s_2. Corresponding equations for defining boundaries are achieved from mass balance equation as follows (for this purpose the mechanical erosion is assumed negligible) [15,21]:

$$\frac{\partial m}{\partial t} = m_\mathrm{p}|_y - m_\mathrm{p}|_{y+\Delta y} = m_\mathrm{p}|_y - m_\mathrm{p}|_y + \frac{\partial}{\partial y}(m_\mathrm{p}\,\Delta y) \tag{7}$$

$$\Rightarrow \frac{\partial}{\partial t}(\rho\,\Delta y) = \frac{\partial}{\partial y}(m_\mathrm{p}\,\Delta y) \tag{8}$$

Therefore:

$$m_\mathrm{p} = \int \frac{\partial \rho}{\partial t}\,\mathrm{d}y \tag{9}$$

The pyrolysis surface position is obtained as follows:

$$s_2(t) = \int_0^t \frac{m_\mathrm{p}}{\rho - \rho_3}\,\mathrm{d}t \tag{10}$$

And a relationship between the top of the char region and the polymer pyrolysis interface can be found [16,18,21]:

$$s_1(t) = s_2(t) + \phi(L_0 - s_2(t)) \tag{11}$$

In Eq. (11) [19,21]:

$$\phi = y_\mathrm{c}\frac{\rho}{\rho_3} \tag{12}$$

To complete the system of equations of the in-depth ablation model, it is essential to include equations for calculation the pyrolysis mass flow rate, m_p. The motion of the pyrolysis zone is defined by the kinetics of resin decomposition.

As mentioned earlier, it is assumed that the rate of decomposition is expressed by the first order reaction [15,21] and the mechanism of polymer degradation is single step:

$$-\frac{\partial[\rho(\nu_2 X_\mathrm{g} - V_\mathrm{gas})]}{\partial t} = k\rho(\nu_2 X_\mathrm{g} - V_\mathrm{gas}) \tag{13}$$

where $(\nu_2 X_\mathrm{g} - V_\mathrm{gas})$ represents the mass ratio of decomposed resin to the virgin resin. Using the Arrhenius type reaction rate constant, equations for calculation m_p are obtained as follows [21,22]:

$$m_\mathrm{p}(t) = \int_0^{\delta_\mathrm{B}} \frac{\partial(\rho V_\mathrm{gas})}{\partial t}\,\mathrm{d}y = \int_0^{\delta_\mathrm{B}} \rho A(\nu_2 X_\mathrm{g} - V_\mathrm{gas}(y,t))\,\mathrm{e}^{-E/RT(y,t)}\,\mathrm{d}y \tag{14}$$

In Eq. (14), the following relations were experimentally determined by Kanevce [22] for X_g of resol type phenolic resin matrix: $X_\mathrm{g}(T) = -0.21322 \times 10^{-6} \times T^2 + 0.80560 \times 10^{-3} \times T - 0.12527$ for $T < 1255\,\mathrm{K}$

$$X_\mathrm{g}(T) = 0.55 \quad \text{for } T \geq 1255\,\mathrm{K} \tag{15}$$

For the case of a horizontal specimen exposed to a uniform heat flux from above, production of bubbles is restricted to a thin surface layer of thickness δ_B. The approximate size of δ_B may be estimated by matching the net heat flux at the top surface to the temperature gradient. The result is that [18,24]:

$$\delta_\mathrm{B} \approx \frac{K\,\Delta T_\mathrm{p}}{\varepsilon q_0 + h(T_0 - T_\mathrm{p}) + \varepsilon\sigma(T_0^4 - T_\mathrm{p}^4)}. \tag{16}$$

2.1.1. Initial and boundary conditions

Ablation is a heat and mass transfer process in which a large amount of thermal energy is expended by sacrificial loss of surface material, thus restricting high environmental temperature to the surface region. The heat input from the environment is absorbed, dissipated, and blocked by numerous mechanisms. These are [21,25–30]:

(a) Heat conduction into the material substrate and storage by its effective heat capacity.
(b) Material phase change.
(c) Heat absorption by gases in the material substrate as they percolate to the surface.
(d) Transpiration of gases from the ablating surface into the boundary layer.
(e) Surface and bulk radiation.
(f) Endothermic chemical reactions.

In its simplest form, the energy balance at the ablating surface is [21,29,31]:

$$q_\mathrm{K} = q_\mathrm{e} - q_\mathrm{rw} - q_\mathrm{bL} - q_\mathrm{w} \quad \text{at } y = s_1(t) \tag{17}$$

where:

$$q_\mathrm{K} = -K\frac{\partial T}{\partial y}; \qquad q_\mathrm{e} = h(T_\mathrm{e} - T_0); \qquad q_\mathrm{rw} = \varepsilon\sigma T_\mathrm{w}^4;$$

$$q_\mathrm{bL} = +\gamma_\mathrm{bL} G I^{-1}(q_\mathrm{e} - q_\mathrm{w}); \qquad q_\mathrm{w} = C_\mathrm{p} I(T_\mathrm{w} - T_0);$$

q_bL is a transpiration cooling flux which can be described as follows [21]:

Gaseous products formed by material ablation are injected into the hot boundary layer. In diffusing through this high temperature

environment, the gases absorb heat by sensible temperature rise. The boundary layer is thus increased in thickness, and its original enthalpy or temperature is lowered. Consequently, less heat is transferred from the environment to the ablating surface.

From the theoretical and experimental results on air-to-air injection, a simple correlation formula has been derived for the transpiration number. This formula has been modified for the injection of gaseous products other than air and is given as [21]:

$$\gamma_{bl} = N\left(\frac{Ma}{M_\nu}\right)^p \quad (18)$$

In oxyacetylene flame test, N, M_ν, and p are equal to 0.68–0.72, 16, and 0.55, respectively [21].

$$T(s_2(t), t) = T_p \quad (19)$$

The applied initial conditions for the composite take the general form [21]:

$$T(y, t)|_{t=0} = T(y, 0) = T_0 \quad (20)$$

It is worth bearing in mind that in our analyses through inverse solution technique, the experimentally measured temperature distributions for each section are used as boundary conditions.

2.2. Kinetic models of thermal degradation

The scope of thermal degradation modeling is to determine the kinetic parameters of the thermal degradation of nanocomposite and composite by using thermo-gravimetric analysis. Determining these parameters is essential to calculate the variation of thermophysical properties of the thermoset nanocomposite and composite, also to use the equations mentioned before [19,21,28,29].

2.3. Thermophysical properties

As said before, under high temperature, all of the heat shield properties such as; density, thermal conductivity, and specific heat would change. Therefore, to exact solve the ablation equation (mass and energy balance); it is required to consider the behaviour of these properties during thermal degradation and ablation by employing some methods which were introduced in the previous works [21,26].

3. Experimental

3.1. Materials

A resol type phenolic resin (IL800/2) supplied from Resitan Company. Properties of this resin are given below [21]:

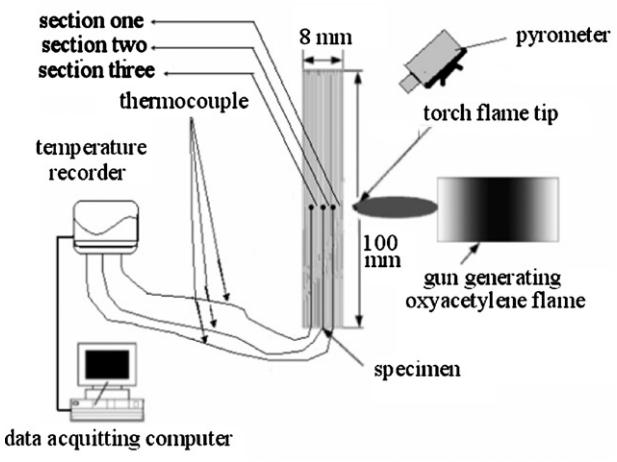

Fig. 2. The oxyacetylene flame test setup.

Density = 1050 kg m^{-3}, gasification coefficient = 0.6, specific heat = 2000 J kg^{-1} K^{-1}, and thermal conductivity = 0.35 J m^{-1} s^{-1} K^{-1}.

Asbestos cloth (Grade AAA) was added as reinforcing to the polymeric matrix. Properties of asbestos cloth are given below [21]:

Thickness = 2 mm, density = 2000 kg m^{-3}, specific heat = 787 J kg^{-1} K^{-1}, and thermal conductivity = 0.65 J m^{-1} s^{-1} K^{-1}.

The montmorillonite sample employed in this work was cloisite 15A from Southern Clay Products, Inc., U.S.A.

3.2. Characterization of polymer layered silicate nanocomposites

The structure of the polymer layered silicate nanocomposites has traditionally been elucidated using X-ray diffraction (XRD) and transmission electron microscopy (TEM) [30]. The most straightforward method is XRD. The sample preparation is relatively easy and the X-ray analysis can be performed within a few hours. Transmission electron microscopy is a useful complement to X-ray diffraction. TEM gives a direct measure of the spatial distribution of the layers but it requires substantial skills in specimen preparation and analysis [6,30,31]. In some cases the TEM cannot give any further information due to the presence of the other fillers such as fibers. In our case, due to the presence of asbestos fabric reinforcement which is the major part of the specimen, TEM cannot give any distinguishable picture of the clay exfoliated layers.

To analyze the samples, XRD a Miniflex diffractometer using Cu-Kα radiation with a dwell time of 1°/min, in the 2θ Bragg-Brentano geometry was employed. STA 625, Polymer Laboratories (TG and TGA) was used to evaluate the thermal performance of

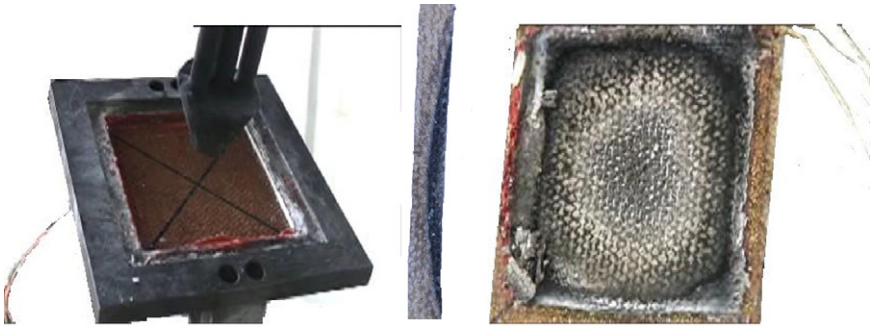

Fig. 3. The sample for the oxyacetylene flame test: (a) before and (b) and (c) after test.

the samples of the insulation material. Moreover, differential scanning calorimeter (DSC PL) was used to calculate the heat of ablation and specific heat. The specific heat capacity measurements were performed according to ASTM D-1269. A heating rate of 10 K/min was used. The thermal conductivity through its thickness was measured by employing a comparative steady state method against a reference sample according to ASTM E1225-87.

To evaluate the thermal behaviour and ablation performance of the ablative material heat shields, the oxyacetylene flame test was carried out according to ASTM-E-285-80. This test can create hot gas with 3400 K and 9×10^6 W/m^2 heat flux. Hot combustion gases are directed along the normal to the specimen. The results of the test are useful to show the thermal behaviour of ablative materials. This test method covers the screening of ablative materials to determine the relative thermal insulation effectiveness when are tested as a flat panel in an environment of a steady flow of hot gas provided by an oxyacetylene burner. The setup of oxyacetylene flame test is demonstrated in Fig. 2.

Cone calorimetry was performed on an Atlas CONE2 according to ASTM E 1354 at a heat flux of 8×10^4 W/m^2. It is a normal irradiance level for the evaluation of the flammability, using a cone shaped heater. Scanning electron microscopy (SEM) studies were carried out using a Philips microscope with a field emission gun operating normally at 20 kV acceleration voltages. The samples were coated with gold/palladium films to a thickness of 2–3 nm using a Denton Magnetron Sputter coater system.

3.3. Sample preparation

In this work, the combination of solution and in situ intercalation methods was used to fabricate the nanocomposite samples. Ethyl alcohol was used to disperse the layered silicates and at the same time, dissolved the phenolic resin. The crystallite delaminated in an excess of ethyl alcohol due to the weak van der Waals force holding the layer together in a stack. Phenolic resin then could be adsorbed onto the delaminated individual layer. However, upon ethyl alcohol removal, the layers could reassemble to reform the stack with phenolic chains sandwich in between, forming a well order intercalated nanocomposites.

Asbestos cloth impregnated by phenolic resin/layered silicate intercalated. The sample was pre-cured at 120 °C for 10 min, and then cured at 160 °C for an hour in autoclave. After curing, the sample was post-cured for half an hour at 150 °C. Therefore, samples were formed due to ethyl alcohol removal and phenolic resin polymerisation. The sample was a flat panel laminate structure by dimensions of 8 mm × 100 mm × 100 mm. Performing oxyacetylene flame test, the nickel-chrome thermocouples were placed through the thickness of the sample, Fig. 3.

The sample for surface erosion measurement has a cylindrical shape with 10 and 25 mm in diameter and height, respectively, Fig. 4.

$s_1(t)$ is equal to the height of cylindrical sample after flame test, which can be directly measured. $s_2(t)$ is also an *equivalent height* of the sample after flame test which is experimentally determined as follow [21]:

$$s_2(t) = \frac{(m_0 - m(t))}{\rho \cdot S} \quad (21)$$

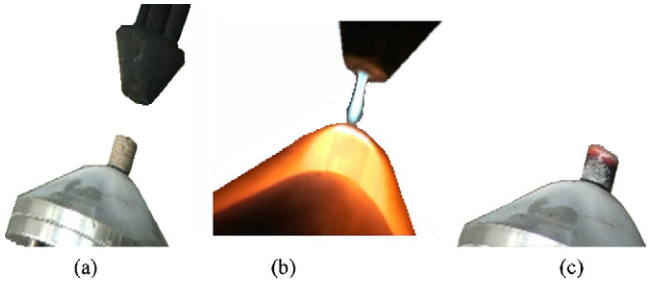

Fig. 4. Measuring the surface erosion by the oxyacetylene flame test: (a) before, (b) due to, and (c) after test.

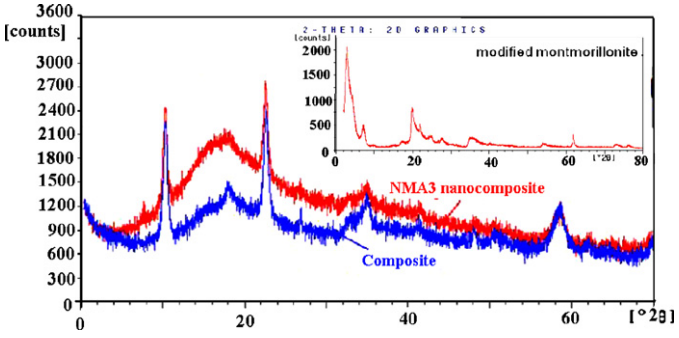

Fig. 5. Comparative X-ray diffraction patterns of composite and NMA3 nanocomposite samples with modified montmorillonite.

Table 2
The d_{001} basal interplanar spacing and 2θ analysis of XRD test.

Sample	d_{001} (Å)	2θ (°)	Δd_{001} (Å)	$\Delta 2\theta$ (°)
Modified Montmorillonite	31.5	2.7	–	–
Nanocomposite (NMA3)	143.52	0.615	112.02	−2.085

The characteristics of the samples are given in Table 1.

4. Results and discussion

4.1. Evaluation the nanocomposite structure

Comparative X-ray diffraction (XRD) patterns of nanocomposite NMA3 and its composite counterpart are presented in Fig. 5. No peaks could be traced; which means the nanocomposite exhibits an exfoliated morphology.

Table 2 shows the XRD analysis results of 0 0 1 *d*-spacing and 2θ for modified montmorillonite and NMA3 nanocomposite. In NMA3 nanocomposite, basal reflection (d_{001}) peak was shifted to lower angle and decreased strongly. Variation in the interplanar spacing was determined by subtracting the basal lattice value of the NMA3 nanocomposite from the basal lattice value of montmorillonite.

4.2. Thermo-gravimetric analysis

Fig. 6 shows a TGA thermogram of weight loss as a function of temperature for phenolic/asbestos composite and nanocomposites

Table 1
The characteristics of the samples.

Sample	*Component*	Resin mass fraction	Clay mass fraction	Asbestos mass fraction
Composite	Asbestos Cloth/Phenolic Resin	0.50	0.00	0.50
Nanocomposite (NMA1)	Asbestos Cloth/Phenolic Resin/Montmorillonite	0.47	0.03	0.50
Nanocomposite (NMA2)	Asbestos Cloth/Phenolic Resin/Montmorillonite	0.44	0.04	0.52
Nanocomposite (NMA3)	Asbestos Cloth/Phenolic Resin/Montmorillonite	0.42	0.06	0.52

Table 3
The kinetic parameters of the samples.

Kinetic parameter	Unit	Phenolic resin (in nitrogen) [21]	Composite (in nitrogen) [21]	Composite (in air)	Nanocomposite (NMA3) (in air)
Activation energy, E	J/mol	1.43×10^5	1.75×10^8	9.57×10^7	10.5×10^7
The difference in activation energy for volatile and char formation, $E_g - E_c$	J/mol	4.1×10^4	3.92×10^7	1.01×10^7	1.3×10^7
Frequency factor, A	s^{-1}	3×10^9	1.26×10^{10}	8.82×10^4	2.8×10^4
The fraction of frequency factor for volatile and char formation, A_g/A_c	–	13	46.5	4	4.3
Degree of thermal degradation reaction, n	–	1	6.5	1.7	1.7

(NMA1, NMA2, and NMA3) under air atmosphere. In general, major weight losses are observed in the temperature range of ~300–500 °C for all of the specimens. It is obvious the presence of clay improves the thermal stability of nanocomposites. Several factors are generally contributed to this improvement. First, a higher energy is required to initiate chain scission as a result of the restricted chain motion in the confined environment. Second, the dispersed large aspect ratio platelets hinder the outward diffusion of the decomposed volatile products, as a direct result of decreased permeability. For thermal oxidation process, the mass transfer of oxygen into the gallery may also be retarded, causes further decreasing in degradation. Evidently, the thermal decomposition of the phenolic/asbestos-montmorillonite nanocomposites shift slightly toward the higher temperature range than of phenolic/asbestos composite, which confirms the enhancement of thermal stability of nanocomposite.

In the following the thermal degradation and ablation performance of composite and NMA3 nanocomposite are investigated which show the lowest and highest thermal stability, respectively.

By considering the methods of calculation and evaluation of thermal degradation kinetic parameters given in our previous work [21,28,29], all of the kinetic parameters of thermal degradation and physical and thermophysical properties of samples were determined and presented in Tables 3 and 4, respectively.

Fig. 7 shows the change of specific heat capacity of the asbestos cloth/phenolic matrix composite in comparison with the NMA3 nanocomposite under heating. Measurement of the specific heat capacity during the polymeric matrix degradation is impossible due to instantaneous sample mass change. Therefore under 500 K, the change of specific heat of the asbestos cloth/phenolic matrix composite and the NMA3 nanocomposite are in the range of 1000–1500 and 3300–5800 $J\,kg^{-1}\,K^{-1}$, respectively. The greater value of the

Table 4
The physical and thermophysical properties of asbestos cloth/phenolic resin composite and nanocomposite at standard conditions.

Properties*	Unit	Composite	Nanocomposite (NMA3)
Density	$kg\,m^{-3}$	1450	1520
Density of pyrolysis gas	$kg\,m^{-3}$	0.3	0.3
Density of char	$kg\,m^{-3}$	1089	1174
Specific heat capacity of char	$J\,kg^{-1}\,K^{-1}$	773	2138
Specific heat capacity	$J\,kg^{-1}\,K^{-1}$	1270	3562
Thermal conductivity	$J\,m^{-1}\,s^{-1}\,K^{-1}$	0.5	0.41
Thermal conductivity constant	–	1.5	1.5

*All of the test methods are described in reference [21].

NMA3 nanocomposite is one of the key factors to cause the higher insulation performance than asbestos cloth/phenolic resin composite.

The under curve surface area of DSC curves of asbestos cloth/phenolic resin composite and NMA3 nanocomposite in Fig. 8 are equal to the heat of ablation (ΔH_p), which are 952 and 45.4 kJ/kg, respectively.

4.3. Ablation performance

After 20 s of the oxyacetylene flame test at 3400 K hot gas temperature and 9×10^6 W/m^2 heat flux, the theoretical values of the char and pyrolysis surface erosion are 1.35 and 1.77 mm for composite and 0.62 and 0.98 mm for NMA3 nanocomposite, respectively. The experimental values of these parameters were 1.9 and 2.6 mm for composite and 1.3 and 2.1 mm for NMA3 nanocomposite, respectively. The differences between experimental and theoretical values

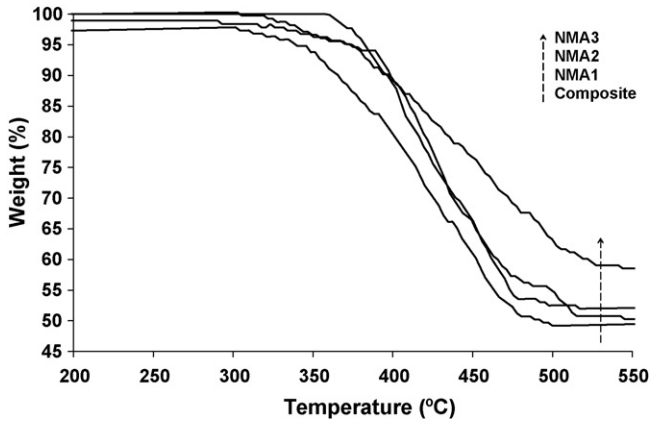

Fig. 6. The TGA thermogram of weight loss for phenolic/asbestos composite and NMA1, NMA2, and NMA3 nanocomposites under air atmosphere.

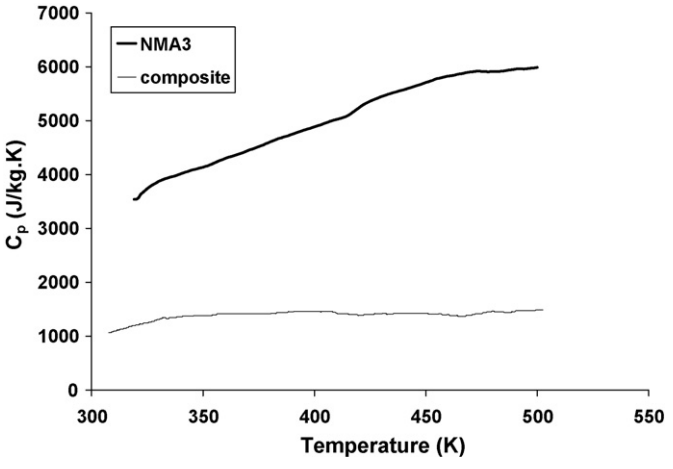

Fig. 7. The specific heat of phenolic/asbestos composite and nanocomposite (NMA3).

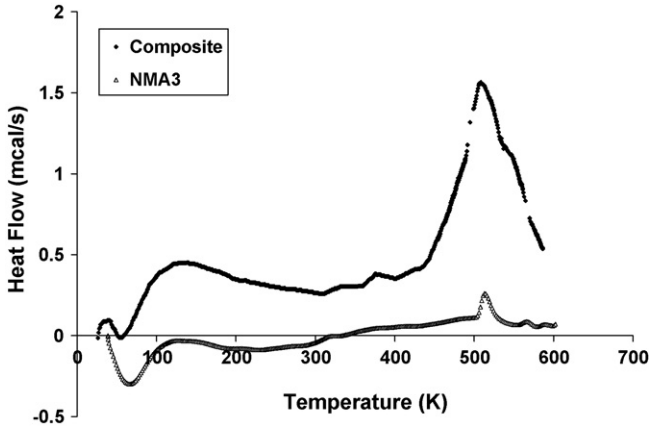

Fig. 8. The DSC curves of phenolic/asbestos composite and nanocomposite (NMA3).

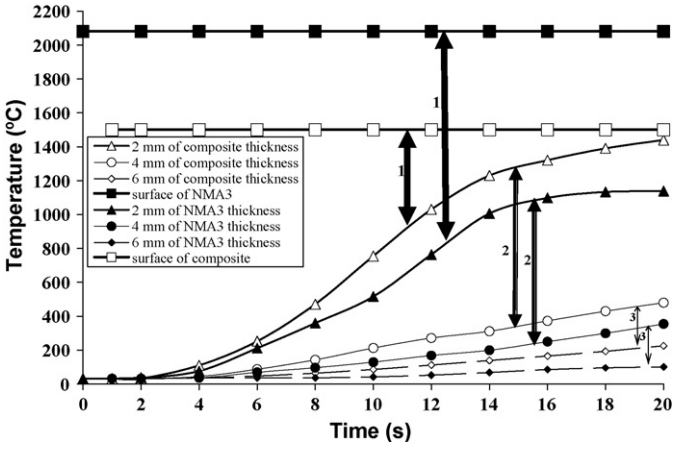

Fig. 9. The experimental temperature distribution of top surface and through the thickness of composite and nanocomposite (NMA3) samples in the oxyacetylene flame test.

are due to abandon the effect of fluid stream force of oxyacetylene flame in the calculation of the surface erosion (Eqs. (10) and (11)).

Fig. 9 shows the experimental temperature distribution of the top surface and through the thickness of asbestos cloth/phenolic

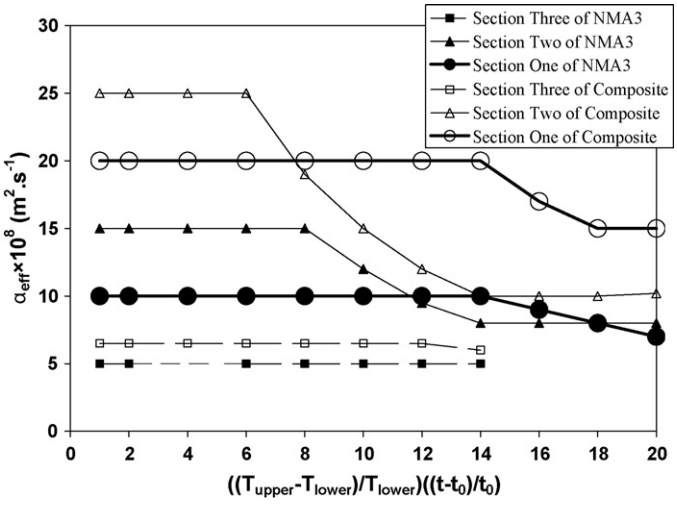

Fig. 10. The change of effective thermal diffusivity in three sections of composite and nanocomposite (NMA3).

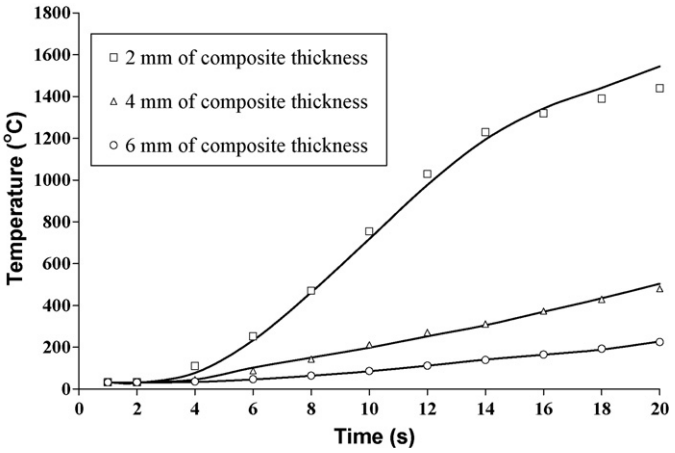

Fig. 11. The temperature distribution through the thickness of composite in the oxyacetylene flame test. Dot points and lines are experimental and theoretical results, respectively.

resin composite and NMA3 nanocomposites in oxyacetylene flame test. Test time duration is 20 seconds. As shown in Fig. 2, three distinct regions were considered through the thickness of the samples. By comparison of these figures it can be observed:

(A) The steady state surface temperature of asbestos cloth/phenolic resin composite and NMA3 nanocomposite are around 1500 °C and 2100 °C in the same condition, respectively. This difference clearly shows that the nature of top surface of composite and nanocomposite are completely different. As known the greater value of surface temperature of the NMA3 nanocomposite is one of the key factors to cause the higher insulation performance than asbestos cloth/phenolic resin composite. Heat radiation flux from nanocomposite surface enhances by increasing the surface temperature.

(B) The difference of temperature profile in section one for both composite and nanocomposite is more than their quantities in sections two and three. In other words, as observed in Fig. 3, under oxyacetylene flame test, the most thermal degradation occurred in section one of the composite and nanocomposite samples. It means that the most difference between ablation performance of composite and nanocomposite is a consequence of thermal degradation, char forming and nature of nanocomposite char layer.

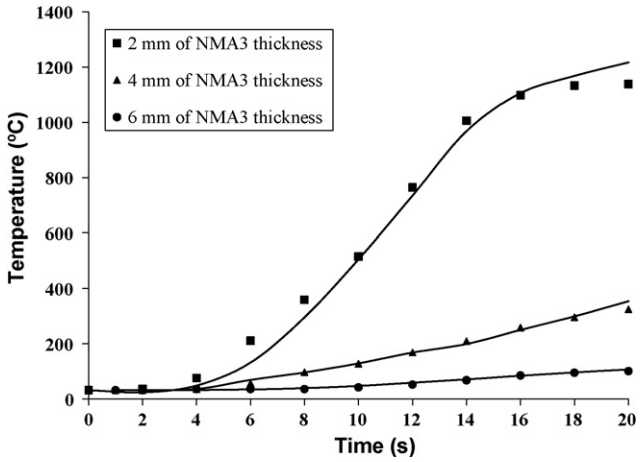

Fig. 12. The temperature distribution through the thickness of nanocomposite (NMA3) in the oxyacetylene flame test. Dot points and lines are experimental and theoretical results, respectively.

4.4. Ablation mechanism

The last section of this work is dedicated to the numerical testing of the simulation model. All the experimental data and model equations obtained are now used in an ablation computer program in order to predict the temperature distribution profile through the thickness of the ablative material as a function of a given heat flux imposed on its external surface. A finite difference method is used to solve the mass and energy balance equations.

Fig. 10 shows the change of effective thermal diffusivity in three sections of both composite and NMA3 nanocomposite samples. These curves were obtained from numerical solution of Eq. (5) by considering the curves of Fig. 9 as boundary conditions. From this figure the following objects are observed:

(a) In the section one that char layer is created due to high temperature ablation, the effective thermal diffusivity of composite is twice than the NMA3 nanocomposite. This phenomenon can lead to a clear difference in char layer nature and ablation mechanism of composite and nanocomposite at high temperature.

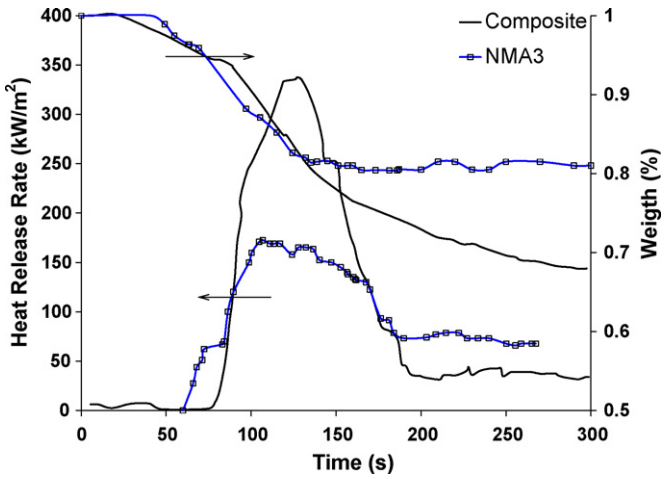

Fig. 13. A comparison of heat release rate and mass loss plot for phenolic asbestos cloth composite and nanocomposite (NMA3) at 80 kW m^{-2} external heat flux.

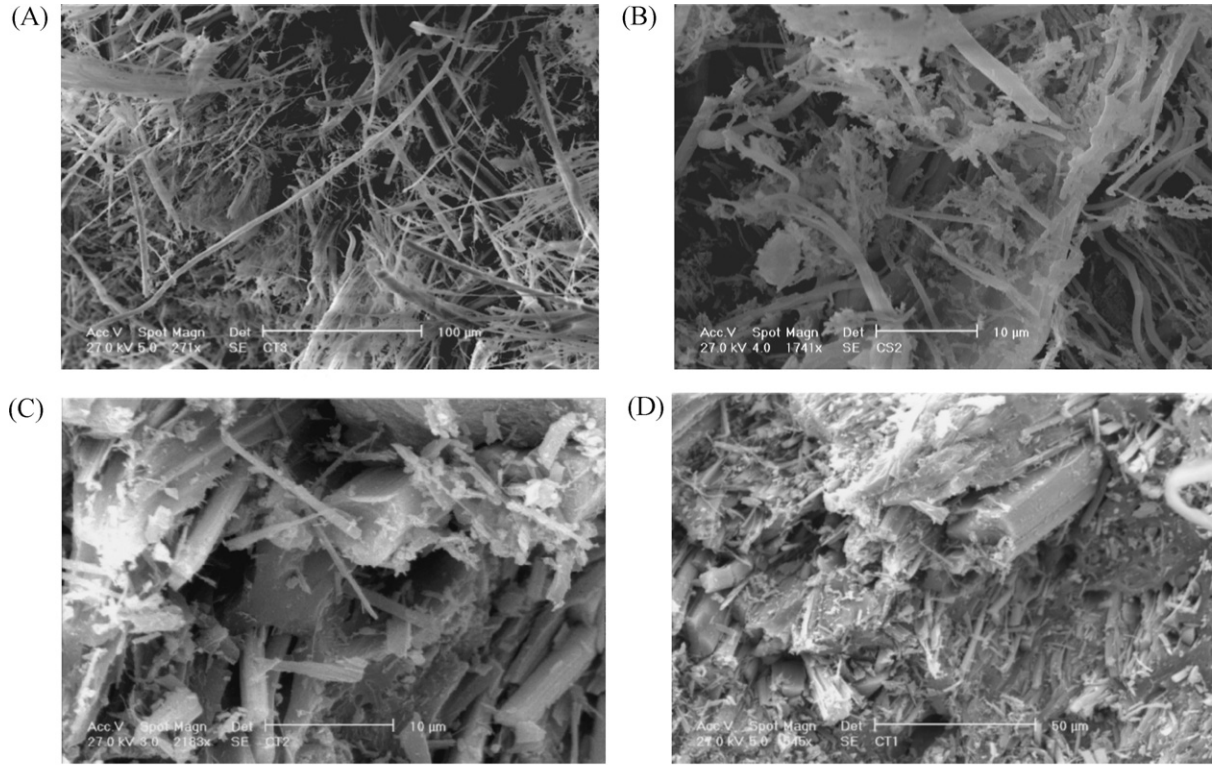

Fig. 14. The scanning electron micrographs of ablative asbestos-phenolic composite after cone calorimetry test. (A) Top surface and (B), (C), and (D) lateral surface, (E) Illustrating of heat flux direction.

(b) The effective thermal diffusivity difference of the sections one and two for composite and nanocomposite is significant while it does not so for the sections three. As shown in Fig. 3, under oxyacetylene flame test the most thermal degradation occurs in the sections one and two of the samples. It means that the most difference between ablation performance of composite and nanocomposite is a consequence of the nature of the nanocomposite char and pyrolysis layers.

(c) As shown in Fig. 2, in the sections three of the samples which remained intact during the oxyacetylene flame test, the effective thermal diffusivity is constant and lower than the others. The effective thermal diffusivity of composite and NMA3 nanocomposite in this section are close enough and equal to $6.5 \times 10^{-8}\,(m^2\,s^{-1})$ and $5 \times 10^{-8}\,(m^2\,s^{-1})$, respectively.

Figs. 11 and 12 show the temperature distribution through the thickness of asbestos cloth/phenolic resin composite and NMA3 nanocomposite samples in oxyacetylene flame test, respectively. In these figures dot points and lines are experimental and theoretical results, respectively. Because of a good agreement between the theoretical and experimental results, the values of effective thermal diffusivity are reliable.

Generally, by considering the results of the oxyacetylene flame test, it concludes that the nanocomposite has a higher ablative performance than composite sample. But this test cannot properly account this feature. The cone calorimetry and scanning electron microscopy are complementary techniques for this purpose.

The heat release rate (HRR) and mass loss plots for asbestos cloth/phenolic composite and NMA3 nanocomposites at $8 \times 10^4\,W/m^2$ external heat flux are shown in Fig. 13. NMA3 nanocomposite shows 51% HRR and 40% mass loss lower than the asbestos cloth/phenolic composite.

Figs. 14 and 15 show scanning electron micrographs of the top surface of the asbestos-phenolic composite and NMA3 nanocomposite samples after cone calorimetry test, respectively. These figures clearly illustrate the char surfaces of the samples. The microstructure of nanocomposite char (Fig. 15) indicates that increasing clay content results in a tougher char. Generally, the spatially uniform arrangement of the silicate layers on an ultra-fine nanometer level facilitates the formation of a uniform inorganic ceramic layer. This dense ceramic layer enhances the ablation performance of nanocomposites at higher temperature.

Fig. 16 shows the X-ray diffraction patterns of composite and NMA3 nanocomposite samples prior to flame test and afterwards.

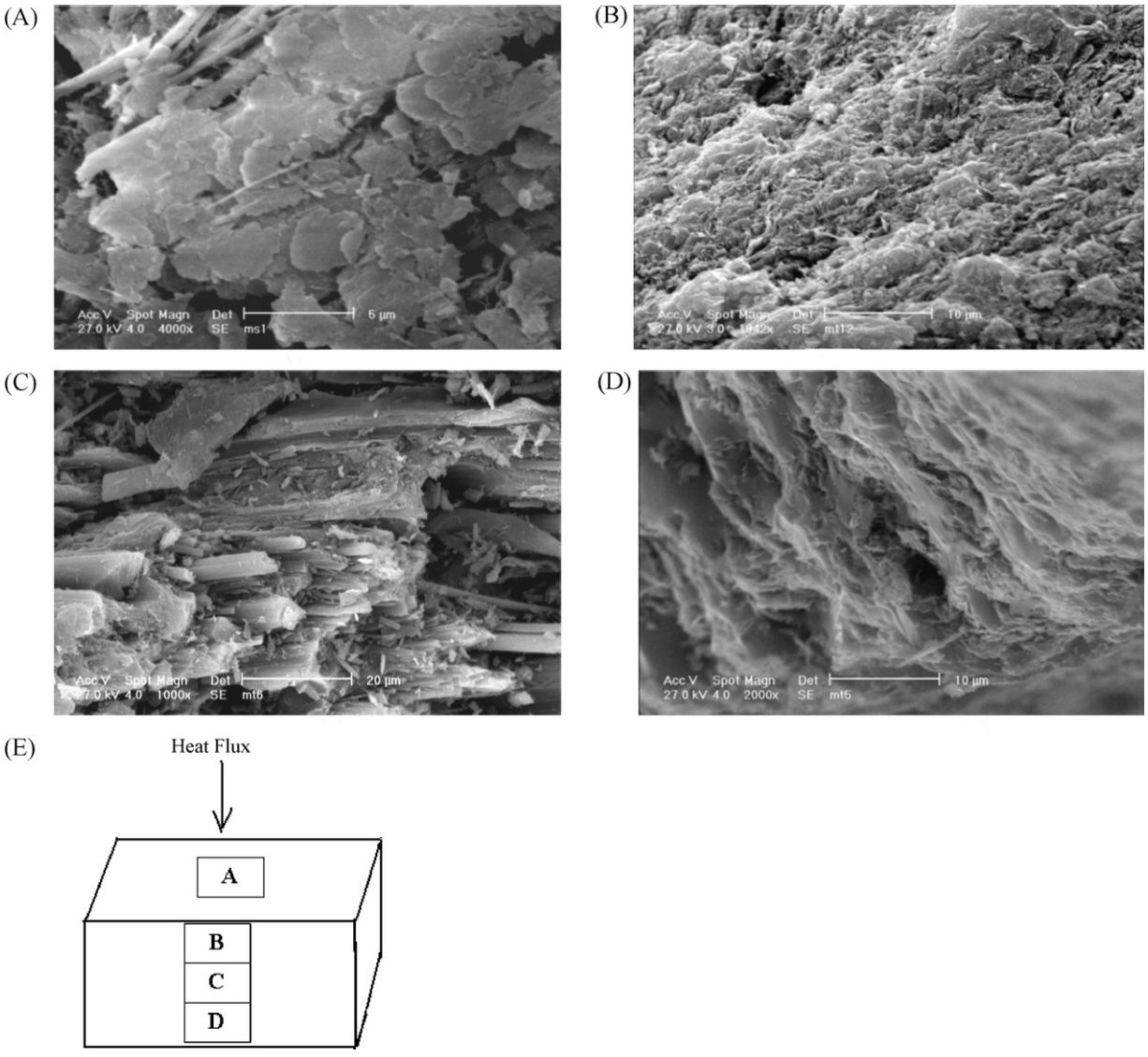

Fig. 15. The scanning electron micrographs of ablative nanocomposite (NMA3) after cone calorimetry test. (A) Top surface and (B), (C), and (D) lateral surface, (E) Illustrating of heat flux direction.

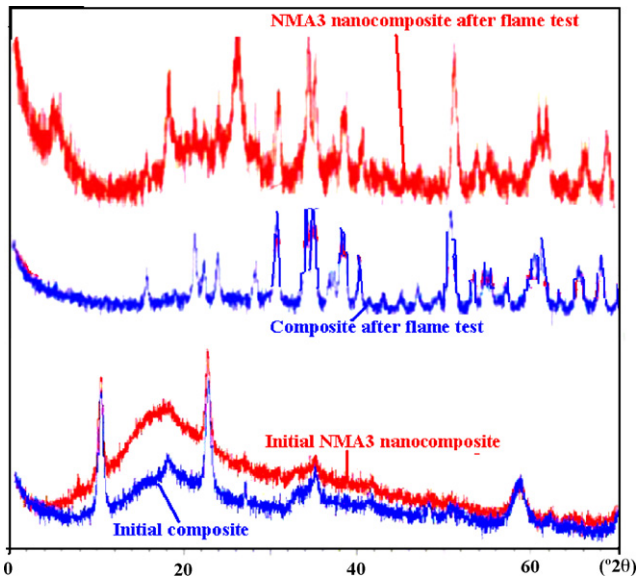

Fig. 16. The X-ray diffraction patterns of composite and NMA3 nanocomposite samples prior to the flame test and afterwards.

The analysis implies that the mineral composition of composite sample changes from Clinochrysotile ($Mg_3Si_2O_5(OH)_4$) to Forsterite (Mg_2SiO_4), after flame test. For NMA3 nanocomposite sample, the composition contains both Forsterite (Mg_2SiO_4) and sodium aluminum silicate ($NaAlSiO_4$), at the end of flame test. So, the char layer of ablative nanocomposite sample contains ceramic based on aluminum silicate.

5. Conclusions

The present research looks at the ablation and thermal properties of resol type phenolic resin/asbestos cloth–clay nanocomposites synthesised by solution and in situ polymerisation of a prepolymer. The inorganic phase was montmorillonite, exchanged with alkylammonium ions in order to give organophilic properties to the phyllosilicate.

The polymer layered silicate nanocomposites results improvement in ablative performance relative to the polymeric composite. A relatively tough, inorganic ceramic layer is formed during ablation of the nanocomposites. This refractory ceramic creates the secondary heat shield to protect the initial heat shield system. According to the nanocomposite heat shield ablation mechanism that illustrated in this work, the main results of thermal stability and ablation performance are given as follow:

1. At 9×10^6 W/m^2 external heat flux and 3400 K temperature of hot gas conditions, the effective thermal diffusivity of resol type phenolic resin-asbestos cloth composite and montmorillonite layered silicate nanocomposites (6% by weight organoclay) estimated. In these test conditions, the ablation performance of NMA3 nanocomposite heat shield is 100% more than composite counterpart.
2. In cone calorimetry test at 8×10^4 W/m^2 radiation external heat flux, the NMA3 nanocomposite shows 51% HRR and 40% mass loss lower than the asbestos cloth-phenolic resin composite.

Acknowledgement

The authors would like to acknowledge all of the corresponding sponsors of this work.

References

[1] J.L. Capitaneo, F.T. Silva, V.R. Caffarena, Aluminosilicate nanocomposite material, Appl. Mineral. 1 (2004) 45–48.
[2] F. Dabrowski, S. Bourbigot, R. Delobel, M.L. Bras, Kinetic modeling of the thermal degradation of polyamide-6 nanocomposite, Eur. Polym. J. 36 (2000) 273–284.
[3] J. Zhang, D.D. Jiang, C.A. Wilkie, Fire properties of styrenic polymer clay nanocomposites based on an oligomerically-modified clay, Polym. Degrad. Stab. 91 (2006) 358–366.
[4] N. Sheng, M.C. Boyce, D.M. Parks, Multiscale micromechanical modeling of polymer/clay nanocomposites and the effective clay particle, Polymer 45 (2004) 487–506.
[5] A. Gultek, T. Seckin, Poly, (methacrylic) acid and methacryloxy propyltrimethoxy silane/clay nanocomposites prepared by in-situ polymerization, Turk. J. Chem. 26 (2002) 925–937.
[6] D. Deana, R. Walkerb, M. Theodoreb, E. Hamptonb, E. Nyairo, Chemorheology and properties of epoxy/layered silicate nanocomposites, Polymer 46 (2005) 3014–3021.
[7] J.L. Capitaneo, F.T. Silva, V.R. Caffarena, Preparation of layered polyvinyl chloride (PVC)-kaolinite nanocomposite, Appl. Mineral. 1 (2004) 53–56.
[8] J.K. Pandey, K.R. Reddy, A.P. Kumar, R.P. Singh, An overview on the degradability of polymer nanocomposites, Polym. Degrad. Stab. 88 (2005) 234–250.
[9] T.B. Tolle, D.P. Anderson, Morphology development in layered silicate thermoset nanocomposites, Composites Sci. Technol. 62 (2002) 1033–1041.
[10] M.C. Costache, D. Wang, M.J. Heidecker, E. Manias, C.A. Wilkie, The thermal degradation of poly (methyl methacrylate) nanocomposites with montmorillonite, layered double hydroxides and carbon nanotubes, Polym. Adv. Technol. 17 (2006) 272–280.
[11] R.A. Vaia, G. Price, P.N. Ruth, H.T. Nguyen, J. Lichtenhan, Polymer/layered silicate nanocomposites as high performance ablative materials, Appl. Clay Sci. 15 (1999) 67–92.
[12] S. Duquesnea, C. Jamaa, M.L. Brasa, R. Delobelb, P. Recourtc, J.M. Gloaguend, Elaboration of EVA–nanoclay systems characterization, Composites Sci. Technol. 63 (2003) 1141–1148.
[13] A. Singh, High-temperature polymer/inorganic nanocomposites, United States Patent, May 2000; 6057035.
[14] J. Zhu, P. Start, K.A. Mauritz, Thermal stability and flame retardancy of poly(methyl methacrylate)-clay nanocomposites, Polym. Degrad. Stab. 77 (2002) 253–258.
[15] L. Torre, J.M. Kenny, A.M. Maffezzoli, Degradation behaviour of a composite material for thermal protection systems, part II process simulation, J. Mater. Sci. 33 (1998) 3145–3149.
[16] J.E.J. Staggs, Simple mathematical models of char forming polymers, Polym. Int. 49 (2000) 1147–1152.
[17] J.E.J. Staggs, A simple model of polymer pyrolysis including transport of volatiles, Fire Saf. J. 32 (1999) 17–34.
[18] S.D. Watt, J.E.J. Staggs, A.C. McIntosh, J. Brindley, A theoretical explanation of the influence of char formation on the ignition of polymers, Fire Saf. J. 36 (2001) 421–436.
[19] R.E. Lyon, Pyrolysis kinetics of char forming polymers, Polym. Degrad. Stab. 61 (1998) 201–210.
[20] C.L. Resch, Ablation models of thermal protection materials, Johns Hopkins APL Technical Digest 13 (1992) 426–431.
[21] A.R. Bahramian, M. Kokabi, M.H.N. Famili, M.H. Beheshty, Ablation and thermal degradation behaviour of a composite based on resol type phenolic resin; process modeling and experimental, Polymer 47 (2006) 3661–3673.
[22] L.D. Kanevce, G.H. Kanevece, Comparison of two kinds of experiments for estimation of thermal properties of ablative composite, in: 3rd International Conference on Inverse Problems in Engineering, June 13–18, Port Ludlow, Washington, USA, 1999.
[23] Y.I. Dimitrienko, I.D. Dimitrienkov, Effect of thermo-mechanical erosion on heterogeneous combustion of composite materials in high-speed flows, Combust. Flame 122 (2000) 211–226.
[24] J.E.J. Staggs, A simplified mathematical model for the pyrolysis of polymers with inert additives, Fire Saf. J. 32 (1999) 221–240.
[25] A.R. Bahramian, M. Kokabi, M.H. Beheshty, M.H.N. Famili, Comparison of thermal degradation of a phenolic matrix composite in air and inert gas, in: 4th International and 7th National Seminar on Polymer Science and Technology, Tehran, Iran, September 27–29, 2005.
[26] Y.I. Dimitrienkov, Effect of finite deformations on internal heat-mass transfer in elastomer ablating materials, Int. J. Heat Mass Transfer 40 (1997) 699–709.
[27] R. Zong, Y. Hu, S. Wang, L. Song, Evaluation of PC/ABS/montmorillonite nanocomposites, Polym. Degrad. Stab. 83 (2004) 423–428.
[28] A.R. Bahramian, M. Kokabi, M.H. Beheshty, M.H.N. Famili, Thermal degradation process of resol type phenolic matrix/kaolinite layered silicate nanocomposite, Iranian Polym. J. 16 (2007) 375–387.
[29] A.R. Bahramian, M. Kokabi, M.H. Beheshty, M.H.N. Famili, High temperature ablation of kaolinite layered silicate/phenolic resin/asbestos cloth nanocomposite, J. Hazard. Mater. 150 (2008) 136–145.
[30] T. Kashiwagi, R.H. Harris, X. Zhang, R.M. Briber, B.H. Cipriano, S.R. Raghavan, W.H. Awad, J.R. Shieds, Flame retardant mechanism of polyamide 6-clay nanocomposites, Polymer 45 (2004) 881–891.
[31] T.D. Fornes, D.R. Paul, Modeling properties of nylon 6/clay nanocomposites using composite theories, Polymer 44 (2003) 4993–5013.